




Cite this: *Chem. Commun.*, 2019, 55, 1746

Received 13th December 2018,
 Accepted 14th January 2019

DOI: 10.1039/c8cc09847f

rsc.li/chemcomm

Hollow core–shell ZnO@ZIF-8 on carbon cloth for flexible supercapacitors with ultrahigh areal capacitance†

Xiao-Man Cao and Zheng-Bo Han *

Rational design and synthesis of hollow core–shell hetero-structures with high complexity still remains challenging for high-performance supercapacitors. Here, a simple and effective strategy that involves a ‘root-etch-wrap’ process was developed to synthesize hollow core–shell hetero-structured electrodes. Specifically, ZnO hollow spheres take root on carbon cloth *via* an *in situ* growth routine, then are etched to aid the generation of a ZIF-8 shell. As-synthesized hollow core–shell ZnO@ZIF-8 is wrapped by PANI nanocoating, resulting in a flexible conductive porous electrode (denoted as PANI/ZnO@ZIF-8-CC). The optimized electrode exhibits an ultrahigh areal capacitance (4839–3987 mF cm⁻² at 5–30 mA cm⁻²), which is at least 3 times higher than that of PANI-CC and ZnO@ZIF-8-CC owing to the synergistic effect. In addition, a symmetric flexible supercapacitor fabricated by PANI/ZnO@ZIF-8-CC exhibits a high energy density of 0.137–0.0891 mW h cm⁻³ (at a power density of 1.421–23.629 W cm⁻³) and a good long-term cycling ability (87% for 10 000 cycles at 5 mA cm⁻²). All of these results make unique core–shell structured PANI/ZnO@ZIF-8-CC a promising electrode material for advanced energy storage and conversion applications.

Flexible supercapacitors, as an emerging energy storage device for portable and wearable electronics, are urgently needed.¹ One critical issue to construct promising flexible supercapacitors is engineering high-performance electrode materials with excellent mechanical robustness. Therefore, much attention is paid to the rational design and synthesis of hybrid electrodes with unique architectures and morphologies.² In particular, hollow core–shell hetero-structures combining functional outershells with inner voids of the hollow cores provide prominent structural advantages in energy storage applications.³ To be specific, engineering the shells with porous features offers many open pore channels and less diffusion blockage, leading to efficient penetration of the electrolyte into the empty cavity of the hollow structure.⁴

Meanwhile, hollow cavities increase the surface-to-bulk ratio thus increasing the electrolyte–electrode contact areas, leading to more effective ion transport. Furthermore, the inner void of hollow cores can effectively resist the volumetric deformation of electrodes caused by repeated insertion/ejection of electrolyte ions, achieving remarkable capacitance and guaranteeing a stable energy output for the supercapacitor.⁵ The rational choice of the core and shell components makes it possible to design high surface area and high-performance hollow core–shell hetero-structured electrode materials for supercapacitors. So far, precise control and manipulation of the unique hollow core–shell hetero-structures still remain challenging.

Metal–organic frameworks (MOFs), a fascinating class of solid crystalline materials, have been considered as promising candidates for electrode materials due to their intrinsic porous characteristics and extraordinarily large surface area.⁶ In particular, it is possible to produce core–shell structures with MOFs as the core or the shell. Nevertheless, the poor electrical conductivity of most MOFs has limited their application as electrode materials. Several strategies are utilized to improve the electrical conductivity of MOF-based electrodes. Firstly, the common approach is to hybridize MOFs with conductive polymers. This has been demonstrated to be an effective way to integrate the merits of the individual counterparts. For example, PANI-ZIF-67 has been successfully fabricated and it showed an enhanced electrochemical performance.⁷ Another wonderful way is *in situ* growth of metal oxides on substrates as bridges. To date, it has been proven that the method of metal oxide rooting on a substrate is effective to restrain the mechanical shedding and it greatly optimizes the electric connection of the active material to the substrate. Moreover, ‘dead mass’ can be avoided when getting rid of the polymer binders and conductive additives.⁸

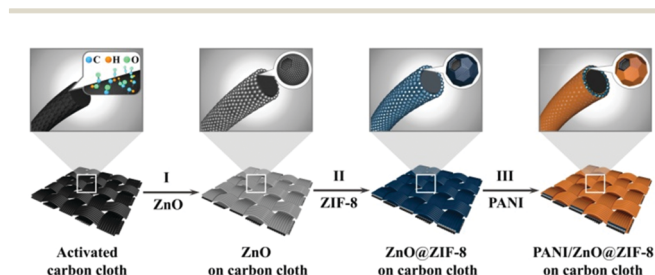
Herein, based on the aforementioned considerations, a unique hollow core–shell hetero-structured electrode (denoted as PANI/ZnO@ZIF-8-CC) is fabricated combining all these strategies into one structure for the first time through a controllable ‘root-etch-wrap’ synthetic strategy. Combining the advantages of the stable structural design and synergistic effects among the components, the

College of Chemistry, Liaoning University, Shenyang 110036, P. R. China.
 E-mail: ceshzb@lnu.edu.cn

† Electronic supplementary information (ESI) available: Experimental details, supporting figures and notes. See DOI: 10.1039/c8cc09847f

electrodes exhibit an ultrahigh areal capacitance of 4839 mF cm^{-2} (at 5 mA cm^{-2}), good rate capability and excellent cycling stability. Our work further demonstrates that hollow core-shell heterostructures can provide huge opportunities and possibilities for high charge-storage capability, and presents PANI/ZnO@ZIF-8-CC holding great promise as a flexible electrode material for advanced energy storage and conversion applications.

A schematic illustration of the whole fabrication process of PANI/ZnO@ZIF-8-CC is depicted in Scheme 1. Firstly, ZnO hollow spheres took root on activated carbon cloth (CC) *via* an *in situ* growth routine (denoted as ZnO-CC). The ZnO hollow spheres ($< 1 \mu\text{m}$ in diameter) cover uniformly on the surface of each carbon cloth fiber (Fig. 1a). The enlarged SEM image (inset in Fig. 1a) and TEM image (Fig. 1b) clearly indicate the hollow structure. The high-resolution TEM image demonstrates that the ZnO hollow spheres present ordered lattice fringes with a layer spacing of about 0.26 nm , corresponding to the (002) plane of the ZnO hexagonal-wurtzite crystal structure.⁹ Secondly, hollow core-shell ZnO@ZIF-8 (denoted as ZnO@ZIF-8-CC) was controllably synthesized. As seen from Fig. 1c, ZIF-8 shells are assembled by numerous interconnected nano-sized ZIF-8 crystals. The hollow core-shell structure consisting of a ZnO core and ZIF-8 shell with tunable shell thickness can be further confirmed by the



Scheme 1 A schematic illustration of the fabrication process.

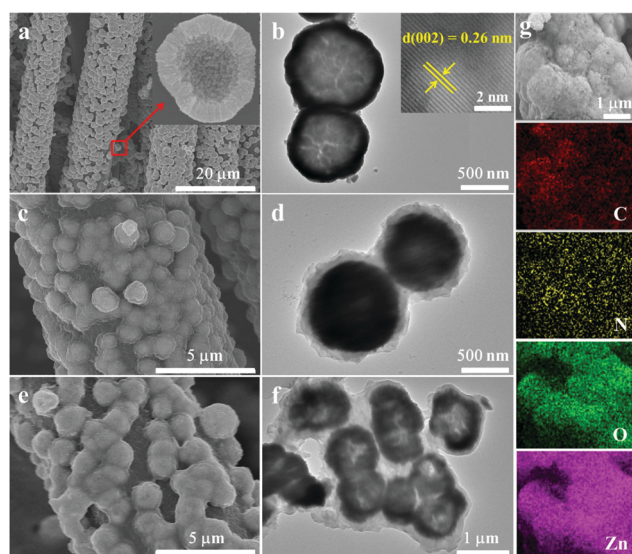


Fig. 1 SEM and TEM images of (a and b) ZnO-CC with corresponding HRTEM image in the inset, (c and d) ZnO@ZIF-8-CC and (e and f) PANI/ZnO@ZIF-8-CC, and (g) elemental mappings for PANI/ZnO@ZIF-8.

contrast of light and shade in the TEM images (Fig. 1d and Fig. S1, ESI[†]). Then, by electropolymerization of aniline, PANI was coated on both the inner and outer surfaces of ZnO@ZIF-8-CC forming a uniform dense nanocoating (denoted as PANI/ZnO@ZIF-8-CC, Fig. 1e). The TEM image further confirms that amorphous PANI is successfully loaded on ZnO@ZIF-8-CC (Fig. 1f). After a three-step assembly, the carbon cloth fiber was completely covered by PANI/ZnO@ZIF-8 and the hollow core-shell structure was well preserved.

X-ray diffraction patterns (XRD) demonstrate the successful integration and maintenance of ZnO@ZIF-8 after electropolymerization (Fig. S2, ESI[†]). PANI/ZnO@ZIF-8-CC is highly hydrophilic in nature with a small contact angle of $\sim 32.9^\circ$ in contrast to 135.3° of ZnO@ZIF-8-CC (Fig. 2a). The hydrophilic groups in PANI/ZnO@ZIF-8-CC mainly include amido ($-\text{NH}-$) and quaternary ammonium (N^+) as evidenced by Fourier transform infrared spectra (FT-IR, Fig. S3, ESI[†]) and X-ray photoelectron spectroscopy (XPS). Both energy-dispersive spectroscopy (EDS, Fig. 1g) and the XPS full-scan spectrum for PANI/ZnO@ZIF-8-CC confirm the existence of C, N, O and Zn elements (Fig. S4, ESI[†]). The high-resolution N 1s spectrum of the samples could be fitted by different electronic states including the quinoid amine ($=\text{N}-$) with the binding energy (BE) centered at 398.7 eV , the benzenoid amine ($-\text{NH}-$) with the BE centered at 399.7 eV , and the positively charged imine ($-\text{N}^+\text{H}-$) and protonated amine ($=\text{N}^+-$) with the BE centered at 400.4 eV and 402.8 eV , respectively, based on the Gaussian fitting method (Fig. 2b).¹⁰ The protonation of PANI is caused by electro-oxidation in the polymerization process. Compared with ZnO@ZIF-8, PANI/ZnO@ZIF-8 reveals an increased ($-\text{NH}-/\text{N}$) ratio from 27.4% to 40.15%, indicating the intrinsic reduction state of PANI (computed by fitting the individual peak areas). For another peak, compared with pure PANI, N^+ shows an upward trend from 11.48% of PANI to 31.91% of the PANI/ZnO@ZIF-8 indicating the increasing protonation level. The results agree well with EDS and FT-IR spectra. Significantly, the electron cloud migration at the ZnO@ZIF-8 and PANI interface leads to a substantial rise of the N valence state, revealing the synergistic effect between ZnO@ZIF-8 and PANI in improving the conductivity. These results confirm that a great number of radical cations are generated after PANI interacted with ZnO@ZIF-8.

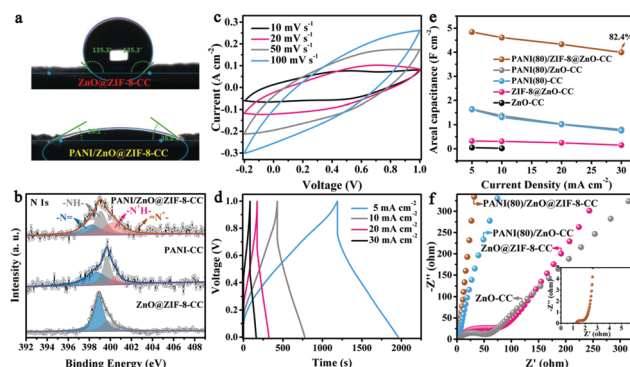


Fig. 2 (a) Contact angles of ZnO@ZIF-8-CC and PANI/ZnO@ZIF-8-CC; (b) N 1s spectrum of the samples; (c) CV and (d) GCD profiles for PANI(80)/ZnO@ZIF-8-CC; (e) areal capacitances and (f) Nyquist plots for the samples with enlarged image of PANI(80)/ZnO@ZIF-8-CC (inset).

In comparison to the ZnO@ZIF-8-CC, the specific surface area (SSA) and pore volume of the PANI/ZnO@ZIF-8-CC are significantly decreased from 185.6 to 136.8 m² g⁻¹ and from 0.116 to 0.104 cm³ g⁻¹, respectively (Fig. S5, ESI[†]). More precisely, the proportion of microporous surface area decreases from 74.4% in ZnO@ZIF-8-CC to 58.6% in PANI/ZnO@ZIF-8-CC, and the ratio of micro-pore volume is decreased from 46.6% in ZnO@ZIF-8-CC to 32.4% in PANI/ZnO@ZIF-8-CC. Compared to ZnO@ZIF-8-CC, which shows a considerable amount of micropores, the PANI/ZnO@ZIF-8-CC exhibits lower SSA due to the introduction of mesopores (that is, generally the SSA tends to decrease with the increase of the pore size). In addition, an important proportion of the in-plane micro-pores are expected to be sacrificed (where PANI and ZnO@ZIF-8 are connected tightly) in PANI/ZnO@ZIF-8-CC, leading to a decreased SSA. This result implies that the intercalated PANI chains do not block the interlayer cavities in the ZnO@ZIF-8-CC and provide extra mesopores in PANI/ZnO@ZIF-8-CC.¹¹

High conductivity combined with large electrolyte-accessible surface area makes PANI/ZnO@ZIF-8-CC an ideal material for flexible energy storage systems. In particular, self-supported PANI/ZnO@ZIF-8-CC can be directly used as an electrode for supercapacitors without any additive. The optimal shell thickness of ZIF-8 and appropriate loading of PANI were determined according to PANI/ZnO@ZIF-8-CC. Firstly, the optimal shell thickness of ZnO@ZIF-8 (*ca.* 100 nm) is selected as the host in the following electropolymerization process of aniline (Fig. S6, ESI[†]). Secondly, the optimized loading of PANI as-obtained by 80 electrodeposition CV segments (PANI(80)/ZnO@ZIF-8-CC) is selected to investigate the electrochemical performance (Fig. S7 and S8, ESI[†]). Typically, the areal mass loading of PANI/ZnO@ZIF-8 is about 6.7 mg cm⁻² and the mass ratio of ZnO/ZIF-8/PANI is *ca.* 5 : 3 : 2. The supercapacitor performance of these electrodes was evaluated under 3 M KCl using a three-electrode cell. The CV curves of activated CC, ZnO-CC, PANI(80)-CC, PANI(80)/ZnO-CC, ZnO@ZIF-8-CC and PANI(80)/ZnO@ZIF-8-CC at the scan rate of 10 mV s⁻¹ are collected in Fig. S9 (ESI[†]). For activated CC and ZnO-CC, the CV areas are negligible, indicating that ZnO@ZIF-8 and PANI serve as the main capacitance contributors. The CV curve of the PANI(80)/ZnO@ZIF-8-CC exhibits a mirror-image current response and the presence of redox reaction peaks, indicating the coexistence of both the EDLC behavior and pseudocapacitance.¹² More importantly, PANI(80)/ZnO@ZIF-8-CC exhibits higher enclosed CV curve area and a higher redox peak intensity compared to the counterparts, revealing a significantly improved specific capacitance and faster redox reaction kinetics processes. The specific capacitance at 10 mV s⁻¹ is only 325.6 mF cm⁻² (61.4 F g⁻¹) for ZnO@ZIF-8-CC, and 1470 mF cm⁻² (810.1 F g⁻¹) for PANI(80)-CC and it increases significantly to 4370 mF cm⁻² (652.2 F g⁻¹) for PANI(80)/ZnO@ZIF-8-CC. It is notable that although PANI(80)/ZnO@ZIF-8-CC exhibits slightly low gravimetric capacitance, its areal capacitance is at least 3 times that of PANI(80)-CC. The enhanced capacitance is derived from the synergistic effect of ZnO, ZIF-8 and PANI, which benefits from the EDLC through high surface area and porosity of ZnO@ZIF-8 and the pseudocapacitance of PANI.

The capacitance surpasses that of PANI-ZIF-67 (2146 mF cm⁻² at 10 mV s⁻¹) by 204%.⁷

A series of CV curves of PANI(80)/ZnO@ZIF-8-CC at different scan rates ranging from 10 to 100 mV s⁻¹ were collected (Fig. 2c). The CV current densities increase linearly with the increase of scanning rates, indicating a good electrochemical reversibility.¹³ The corresponding capacitances of PANI/ZnO@ZIF-8-CC are shown in Fig. S10 (ESI[†]). In addition, the galvanostatic charge-discharge (GCD) curves are slightly distorted from the ideal triangle shape (Fig. 2d), because of the pseudocapacitive contribution from PANI.¹⁴ The maximum areal capacitance of PANI(80)/ZnO@ZIF-8-CC can reach up to 4839 mF cm⁻² at a current density of 5 mA cm⁻². To the best of our knowledge, this is the highest capacitance for all MOF-based electrodes with an aqueous electrolyte under similar testing conditions (Table S1, ESI[†]). Of particular note, when the current density increases up to 30 mA cm⁻², the areal capacitance still remains at 3987 mF cm⁻², which further confirms the excellent rate capability of PANI(80)/ZnO@ZIF-8-CC. In contrast, PANI(80)/ZnO-CC and PANI(80)-CC without a ZIF-8 interlayer only give an areal capacitance of 1658 and 1630 mF cm⁻² at a current density of 5 mA cm⁻², respectively. It can be seen that a more superior capacitance retention rate of 82.4% than those of PANI(80)/ZnO-CC (48.4%) and PANI(80)-CC (46.0%) was obtained from 5 to 30 mA cm⁻² (Fig. 2e), which may be because all hydrophilic PANI is inserted into the pores of ZnO@ZIF-8, which are accessible to the electrolyte and efficiently reduce the 'dead' mass in the electrode.¹⁵ More importantly, the core-shell heterostructure of PANI(80)/ZnO@ZIF-8-CC can still be maintained after the charge-discharge process (Fig. S11, ESI[†]).

The obtained Nyquist plots demonstrate a lower equivalent series resistance of PANI(80)/ZnO@ZIF-8-CC ($R_s = 1.22 \Omega$) than that of ZnO@ZIF-8-CC ($R_s = 6.92 \Omega$), which confirms that the wonderful structure of PANI(80)/ZnO@ZIF-8-CC can accelerate the transport and diffusion of ions and electrons (Fig. 2f). In addition, the straight line of PANI(80)/ZnO@ZIF-8-CC at low frequency is nearly parallel to the imaginary axis, further demonstrating the ideal capacitive performance.⁵

Driven by the increasing requirement for wearable and smart electronic devices,¹⁶ a symmetric flexible supercapacitor device was assembled with PANI(80)/ZnO@ZIF-8-CC and PVA/KCl gel electrolytes sandwiched between the electrodes. The schematic structure and the realistic flexible supercapacitor device are shown in Fig. 3a and Fig. S12a (ESI[†]). The CV curves of the device based on PANI(80)/ZnO@ZIF-8 have a large closed area and a near rectangular shape at a scan rate of 1 to 50 mV s⁻¹ (Fig. S12b, ESI[†]). The GCD measurement of the device is presented in Fig. S12c (ESI[†]). Based on the GCD curves at 0.5–5 mA cm⁻², the device exhibits the areal capacitance of 226.9–147.5 mF cm⁻² (986.5–641.3 mF cm⁻³). The high energy densities of 0.0315–0.0205 mW h cm⁻² (0.137–0.089 mW h cm⁻³) were achieved at the power densities of 0.327–5.435 W cm⁻² (1.421–23.629 W cm⁻³). The superior capacitance retention (87% for 10 000 cycles at 5 mA cm⁻²) indicates outstanding cycling performance (Fig. 3b). The mechanical stability of the device was evaluated under various mechanical bending angles and its electrochemical performance was investigated by CV curves (Fig. 3c). From the

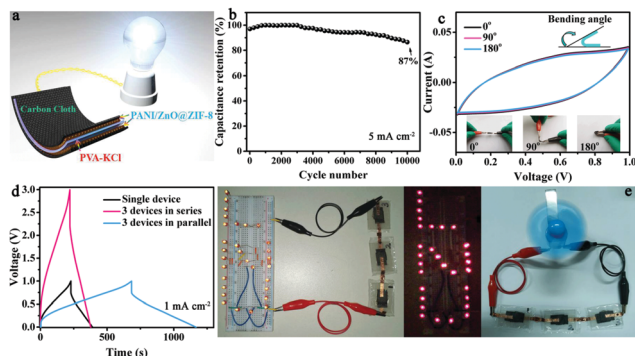


Fig. 3 (a) Schematic representation of the device; (b) cycling test via a GCD cycling process for 10 000 cycles; (c) CV curves of the device at different bending angles; (d) GCD curves of the devices connected in series and in parallel; (e) photographs of three connected devices in series powering a LED lighting matrix and one mini-fan.

CV curves, no obvious changes are seen at angles of 0° , 90° , and 180° , suggesting that the device maintains a very stable performance under the condition of bending. We further explore the potential of the flexible supercapacitor devices for practical applications in series and in parallel (Fig. 3d). Encouragingly, three connected devices in series can successfully power up a LED lighting matrix and drive one mini-fan (Fig. 3e). These results suggest the potential of such MOF-based supercapacitors for flexible and wearable electronics.

Overall, the superior supercapacitive performance of PANI(80)/ZnO@ZIF-8-CC can benefit from the smart hollow core-shell hetero-structure and unique components. The outstanding performance of the PANI/ZnO@ZIF-8-CC electrode can be ascribed to the following points: (i) the intimate connection of ZnO with the substrate can significantly decrease the contact resistance and provide a highly conductive pathway facilitating ion and electron transportation; (ii) the hollow core-shell hetero-structure containing abundant space can effectively accommodate volumetric change during the repeated charge/discharge process, which is significant for restraining structural breakdown and fast capacitance decay of the electrode; (iii) the synergetic effects of ZnO@ZIF-8 and PANI can enhance the capacitance and improve electron conductivity. More specifically, the large surface area and high porosity of ZnO@ZIF-8 can provide abundant adsorption sites and tremendous micropores (≈ 1 nm) that can strongly adsorb electrolyte ions to provide higher EDLC capacitance. Moreover, the prominent electrical conductivity and hydrophilic property of PANI are also beneficial to improve the ion diffusion coefficient; furthermore, PANI can provide extra pseudocapacitance.

In summary, we have developed a 'root-etch-wrap' synthetic strategy to fabricate a hollow core-shell hetero-structured PANI/ZnO@ZIF-8-CC electrode used for high-performance flexible supercapacitors. The unique structure, *in situ* growth strategy of active materials on the substrate and synergistic effects of

each component endow PANI/ZnO@ZIF-8-CC with excellent mechanical robustness, and prominent electrical conductivity, therefore displaying ultrahigh areal capacitances (4839 mF cm^{-2} at 5 mA cm^{-2}), superior rate capability and good cycling stability (87% for 10 000 cycles at 5 mA cm^{-2}). The method presented here is suitable for the development of high-capacitive and mechanically durable supercapacitors, which will provide a new opportunity for enriching applicable MOF-based electrode materials in flexible energy conversion and storage devices.

This work was granted financial support from the National Natural Science Foundation of China (No. 21671090).

Conflicts of interest

There are no conflicts to declare.

Notes and references

- 1 D. P. Dubal, N. R. Chodankar, D. H. Kim and P. G. Romero, *Chem. Soc. Rev.*, 2018, **47**, 2065–2129.
- 2 M. B. Gawande, A. Goswami, T. Asefa, H. Z. Gou, A. V. Biradar, D. L. Peng, R. Zboril and R. S. Varma, *Chem. Soc. Rev.*, 2015, **44**, 7540–7590.
- 3 S. H. Dong, C. X. Li, Z. Q. Li, L. Y. Zhang and L. W. Yin, *Small*, 2018, **14**, 1704517.
- 4 C. Xia, W. Chen, X. B. Wang, M. N. Hedhili, N. N. Wei and H. N. Alshareef, *Adv. Energy Mater.*, 2015, **5**, 1401805.
- 5 L. Yu, H. Hu, H. B. Wu and X. W. Lou, *Adv. Mater.*, 2017, **29**, 1604563.
- 6 (a) P. Q. Liao, J. Q. Shen and J. P. Zhang, *Coord. Chem. Rev.*, 2018, **373**, 22–48; (b) N. Wei, R. X. Zuo, Y. Y. Zhang, Z. B. Han and X. J. Gu, *Chem. Commun.*, 2017, **53**, 3224–3227; (c) Y. Zhang, Y. X. Wang, L. Liu, N. Wei, M. L. Gao, D. Zhao and Z. B. Han, *Inorg. Chem.*, 2018, **57**, 2193–2198; (d) L. Liu, S. M. Wang, Z. B. Han, M. L. Ding, D. Q. Yuan and H. L. Jiang, *Inorg. Chem.*, 2016, **55**, 3558–3565.
- 7 L. Wang, X. Feng, L. T. Ren, Q. H. Piao, J. Q. Zhong, Y. B. Wang, H. W. Li, Y. F. Chen and B. Wang, *J. Am. Chem. Soc.*, 2015, **137**, 4920–4923.
- 8 K. B. Xu, R. J. Zou, W. Y. Li, Q. Liu, X. J. Liu, L. An and J. Q. Hu, *J. Mater. Chem. A*, 2014, **2**, 10090–10097.
- 9 V. Sahu, S. Goel, R. K. Sharma and G. Singh, *Nanoscale*, 2015, **7**, 20642–20651.
- 10 (a) P. P. Li, Z. Y. Jin, L. L. Peng, F. Zhao, D. Xiao, Y. Jin and G. H. Yu, *Adv. Mater.*, 2018, **30**, 1800124; (b) W. P. Kang, Y. Zhang, L. L. Fan, L. L. Zhang, F. N. Dai, R. M. Wang and D. F. Sun, *ACS Appl. Mater. Interfaces*, 2017, **9**, 10602–10609; (c) H. Mei, Y. J. Mei, S. Y. Zhang, Z. Y. Xiao, B. Xu, H. B. Zhang, L. L. Fan, Z. D. Huang, W. P. Kang and D. F. Sun, *Inorg. Chem.*, 2018, **57**, 10953–10960.
- 11 J. Wang, J. Tang, B. Ding, V. Malgras, Z. Chang, X. D. Hao, Y. Wang, H. Dou, X. G. Zhang and Y. Yamauchi, *Nat. Commun.*, 2017, **8**, 15717.
- 12 M. Kim, C. Lee and J. Jang, *Adv. Funct. Mater.*, 2014, **24**, 2489–2499.
- 13 (a) M. Cheng, Y. N. Meng, Q. H. Meng, L. J. Mao, M. Zhang, K. Amin, A. Ahmad, S. X. Wu and Z. X. Wei, *Mater. Chem. Front.*, 2018, **2**, 986–992; (b) Z. Y. Xiao, L. L. Fan, B. Xu, S. Q. Zhang, W. P. Kang, Z. X. Kang, H. Lin, X. P. Liu, S. Y. Zhang and D. F. Sun, *ACS Appl. Mater. Interfaces*, 2017, **9**, 41827–41836.
- 14 J. J. Wu, J. Peng, Z. Yu, Y. Zhou, Y. Q. Guo, Z. J. Li, Y. Lin, K. Q. Ruan, C. Z. Wu and Y. Xie, *J. Am. Chem. Soc.*, 2018, **140**, 493–498.
- 15 K. Zhou, Y. He, Q. C. Xu, Q. E. Zhang, A. A. Zhou, Z. H. Lu, L. K. Yang, Y. Jiang, D. T. Ge, X. Y. Liu and H. Bai, *ACS Nano*, 2018, **12**, 5888–5894.
- 16 (a) F. X. Wang, X. W. Wu, X. H. Yuan, Z. C. Liu, Y. Zhang, L. J. Fu, Y. S. Zhu, Q. M. Zhou, Y. P. Wu and W. Huang, *Chem. Soc. Rev.*, 2017, **46**, 6816–6854; (b) X. M. Cao, Z. J. Sun, S. Y. Zhao, B. Wang and Z. B. Han, *Mater. Chem. Front.*, 2018, **2**, 1692–1699.